Journal of Robotics and Control (JRC)
Volume 6, Issue 1, 2025
ISSN: 2715-5072, DOI: 10.18196/jrc.v6i1.25579

Tracking Iterative Learning Control of TRMS using Feedback Linearization Model with Input Disturbance

Hoang Dang Danh [1], Chi Nguyen Van [2*], Quy Vu Van [3]
[1, 2, 3] Thai Nguyen University of Technology, Vietnam
Email: [1] hoangktd1977@tnut.edu.vn, [2] ngchi@tnut.edu.vn, [3] vuvanquy@tnut.edu.vn
* Corresponding Author

***Abstract*—This paper presents a method for angular trajectory tracking control of the Twin Rotor Multi-Input Multi-Output System (TRMS) experimental model using linearized feedback control with nonlinear compensation and iterative learning-based angular trajectory tracking control. First, the dynamic model of the Twin Rotor MIMO System (TRMS) is developed in the form of Euler-Lagrange (ELF), including descriptions of uncertain parameters and input disturbances such as energy dependence related to the mass of components, friction forces, the effect of the TRMS flat cable, and the impact of the main rotor and tail rotor speeds on horizontal and vertical movements. Based on the nonlinear acceleration equations for the pitch and yaw angles of the TRMS, a compensator is designed to address the nonlinearity of the EL model. Notably, this compensator self-adjusts the compensation signal so that the closed-loop system, consisting of the TRMS and the compensator, becomes a predetermined linear model. Therefore, the structure of the compensator does not need to be designed based on the nonlinear model of the TRMS. After incorporating the compensator, the ELF becomes nearly linear with sufficient accuracy as designed. This system is then controlled using a predefined trajectory tracking controller based on iterative learning with proportional-type learning parameters. By adjusting a sufficiently small optional time parameter, the trajectory tracking error of the pitch and yaw angles of the closed-loop system can be reduced to a desired small-radius neighborhood. Simulation and experimental results demonstrate the trajectory-tracking capability of the closed-loop system. Although the convergence rate depends on the complexity of the TRMS dynamics, the robustness of this method with varying initial conditions is always ensured. The computational complexity is slightly higher compared to other methods, Still, this study contributes a straightforward yet effective trajectory control method under conditions of noise depending on the position, velocity, pitch and yaw angles and unmeasured kinematic model parameters for the TRMS system.**

Keywords*—Feedback Linearization Control; Uncertain Parameters; Iterative Learning; TRMS; Euler-Lagrange Form; Input Disturbances.

I. INTRODUCTION

The TRMS system is manufactured by Feedback Instrument, as illustrated in Fig. 1. Due to the TRMS's rapid and complex nonlinear dynamic properties, its sensitivity to external disturbances, and the challenges in accurately measuring its parameters, the TRMS model is frequently used in laboratory research on control algorithms [1]-[5]. The TRMS is a highly nonlinear system involving vertical and horizontal movements driven by propulsive forces from the main rotor and horizontal tail rotor, respectively, with these forces varying based on the voltages applied to the DC motors. Yaw and pitch angles are measured using tachometers. The angle stabilization control problem for the TRMS is challenging due to its dynamic characteristics, including high nonlinearity and significant coupling between horizontal and vertical motions. In addition, factors such as friction, cable, and gyro moments act as input disturbances affecting the propulsive moments and are difficult to model precisely in practice. Variations in rotor speeds introduce substantial cross-coupling into the system, causing deviations from a flat system behavior [6], [11], [12].

Fig. 1. TRMS apparatus in the Instrument and Control Lab 309 TN Buliding, Thai Nguyen University of Technology

Additionally, obtaining an exact model of the TRMS is challenging because many physical parameters are difficult to measure accurately. Parameters provided by the manufacturer can change over time during practical use of the TRMS, particularly the inertia constant, friction coefficient, viscosity constant, and sign function in the propulsive forces, all of which affect system performance and angle tracking errors. Over the past decade, various tracking control strategies for the TRMS have been explored. References [2] and [3] discussed the use of PID controllers and PID controllers with derivative filter coefficients. References [20]-[23], [15] cover control strategies for the TRMS using fuzzy logic and PID controllers. Reference [4] describes the application of an LQR controller based on the linearized TRMS model in hover mode, while reference [5] discusses an optimal state feedback controller using the LQR technique. References [6]-[10] examine the use of terminal sliding mode control to maintain system stability in pitch and yaw disturbances. Adaptive model inversion control approaches using artificial neural networks and genetic algorithms are presented in references [13], [14], [16]-[19]. The sliding mode control method, known for its robustness in tracking errors, is discussed in references [39], [40], [29] where neural networks are used to approximate the dynamic model in sliding control laws. However, this approach is complex and challenging to implement in practice.

The TRMS, characterized by rapidly changing dynamics, particularly the nonlinear influence of dynamic disturbances and unmeasured parameters on pitch and yaw movements, presents significant challenges. Consequently, PID, LQR, and fuzzy controllers in the aforementioned literature must either disregard these factors during the design process or assume certain limits to incorporate them into the design expressions. These controllers simultaneously perform both trajectory tracking and handling the effects of disturbances and unmeasured parameters within the control law, which limits control quality. Our solution to this issue involves using two control loops: an inner loop with a compensator to linearize the closed-loop system and an outer loop for trajectory tracking with iterative learning to improve tracking errors after each control cycle. Specifically, this study employs a feedback linearization regulator combined with iterative learning techniques [41]-[43] to develop an adaptive controller aimed at stabilizing the yaw and pitch angles of a TRMS. Initially, the mathematical model of the TRMS is reformulated into ELF incorporating uncertain parameters and input disturbances. These disturbances include energy variations dependent on the mass of TRMS components, frictional forces, flat cable tension, the influence of the main rotor's speed on horizontal motion, and the tail rotor's speed on vertical movement. Subsequently, a trajectory control strategy is proposed for the TRMS to handle noise and unmeasured parameters. Utilizing the acceleration equations for the pitch and yaw angles, a compensator is designed to address the nonlinearity present in the Euler-Lagrange model. This compensator is notable for its independence from the TRMS model. Following the integration of the compensator, the Euler-Lagrange system approximates linearity with high accuracy. The closed-loop TRMS system is then controlled using a trajectory tracking controller based on iterative learning with proportional-type learning parameters. By optimizing an adjustable time parameter, the trajectory tracking error for the pitch and yaw angles can be minimized to a desired small vicinity around the target error region [25]-[28]. The research contribution is using linearized feedback control with nonlinear compensation and IL-based angular trajectory tracking control for TRMS model developed in the form of Euler-Lagrange (ELF), including descriptions of uncertain parameters and input disturbances such as energy dependence related.

The structure of this paper is outlined as follows: The subsequent section addresses the reformulation of the TRMS model into ELF, incorporating uncertain parameters and input disturbances. This is followed by the development of a tracking control strategy for the TRMS, which integrates a non-model-based feedback linearization regulator with IL [52]-[55]. Section 4 presents the results derived from experimental studies. The final section provides the conclusions drawn from the research.

II. The Model of TRMS in ELF with Uncertain Parameters and Input Disturbances

The mathematical modeling of the TRMS has been extensively addressed by various authors in seminal works such as those referenced in [2], [3]. In this study, we use the model proposed in [32]-[36], which provides a fairly accurate description of the TRMS dynamics based on the Lagrangian method. This model accounts comprehensively for the forces influencing TRMS motion, including frictional forces, forces exerted by the cables, the effects of the main rotor and the tail rotor speeds on horizontal, and vertical movements, respectively. To represent the TRMS model, we use the following notation: φ_h, φ_v are the horizontal and vertical angles, which are measured outputs; ω_h, ω_v are rotational speeds of tail rotor and main rotor; k_{fhn}, k_{fvp}, k_{fvn}, mT_1, l_{T_1}, mT_2, l_{T_2}, g, h, l_t, l_m, are the physical, and defined parameters k_m, k_g, k_{fhp} of the TRMS are shown in the appendix of this artice. Fig. 2 denotes the parameters used to form the TRMS model. After a thorough examination of the kinematics of the TRMS, we observe that the parameters J_1, J_2 and J_3 are calculated by

$$\begin{aligned} J_1 = \left(\frac{m_t}{3} + m_{tr} + m_{ts}\right) l_t^2 &\\ + \left(\frac{m_m}{3} + m_{mr} + m_{ms}\right) l_m^2 &\\ + \frac{m_{ms}}{2} r_{ms}^2 + m_{ts} r_{tr}^2 &\\ J_2 = \frac{m_b}{3} l_b^2 + m_{cb} l_{cb}^2 &\\ J_3 = \frac{m_h}{3} h^2 & \end{aligned} \tag{1}$$

and they are difficult to measure accurately, therefore, we assume these unknown parameters are represented by the vector $\underline{\theta}$ as described in equation (2):

$$\underline{\theta} = [J_1 \quad J_2 \quad J_3] \tag{2}$$

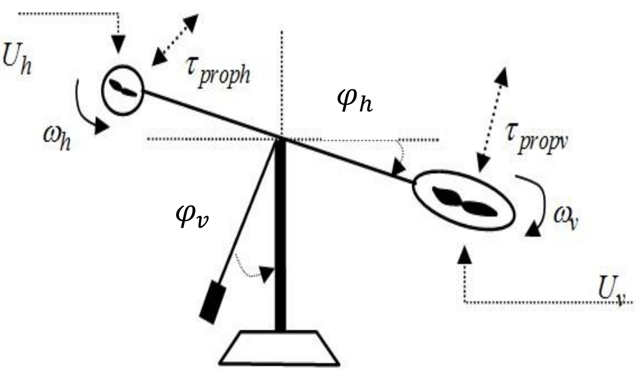

Fig. 2. The symbols used to describe the physical quantities in the TRMS model

To address the trajectory tracking control problem for the angles φ_h and φ_v (which are state variables) of the TRMS, we define the vectors $\underline{\varphi} = [\varphi_h \quad \varphi_v]^T$, $\underline{\dot{\varphi}} = [\dot{\varphi}_h \quad \dot{\varphi}_v]^T$, and $\underline{\ddot{\varphi}} = [\ddot{\varphi}_h \quad \ddot{\varphi}_v]^T$ to represent the state variables, their time derivatives, and their accelerations, respectively. Following the approach outlined in reference [15], we employ the comprehensive kinematic model that incorporates the unknown parameters $\underline{\theta}$, and the forces affecting the TRMS motion, as detailed in Eq (3) below.

$$\boldsymbol{M}(\underline{\varphi},\underline{\theta})\underline{\ddot{\varphi}} + \boldsymbol{C}(\underline{\varphi},\underline{\dot{\varphi}},\underline{\theta})\underline{\dot{\varphi}} + \boldsymbol{G}(\underline{\varphi}) = \underline{\tau} + \underline{\tau}_d \tag{3}$$

where the system matrices and vectors, which are depend on the uncertain parameters vector $\underline{\theta}$, are defined as follows:

$$\boldsymbol{M}(\underline{\varphi},\underline{\theta}) = \begin{bmatrix} \theta_1 \cos^2\varphi_v + \theta_2 \sin^2\varphi_v \\ +h^2\left(m_{T_1} + m_{T_2}\right) + \theta_3 & hm_{T_1}l_{T_1}\sin\varphi_v - \\ & hm_{T_2}l_{T_2}\cos\varphi_v \\ hm_{T_1}l_{T_1}\sin\varphi_v - & \theta_1+\theta_2 \\ hm_{T_2}l_{T_2}\cos\varphi_v & \end{bmatrix} \tag{4}$$

is the generalized inertia matrix, it is also defined positive matrix.

$$\boldsymbol{C}(\underline{\varphi},\underline{\dot{\varphi}},\underline{\theta}) = \begin{bmatrix} 2(\theta_2-\theta_1)\sin\varphi_v\cos\varphi_v\,\dot{\varphi}_v & h\left(m_{T_1}l_{T_1}\cos\varphi_v \right. \\ & \left. +m_{T_2}l_{T_2}\sin\varphi_v\right)\dot{\varphi}_v \\ (\theta_1-\theta_2)\sin\varphi_v\cos\varphi_v\,\dot{\varphi}_h & 0 \end{bmatrix} \in R^{2\times 2} \tag{5}$$

is the centripetal-coriolis matrix.

$$\boldsymbol{G}(\underline{\varphi}) = \begin{bmatrix} 0 \\ g\left(m_{T_1}l_{T_1}\cos\varphi_v + m_{T_2}l_{T_2}\sin\varphi_v\right) \end{bmatrix} \in R^{2\times 1} \tag{6}$$

is gravity vector.

The vector $\underline{\tau} = [\sum_i \tau_{ih} \quad \sum_i \tau_{iv}]^T \in R^{2\times 1}$ represents the total applied torques in the horizontal and vertical directions, where $\sum_i \tau_{ih}$ denotes the sum of torques acting in the horizontal plane, and $\sum_i \tau_{iv}$ represents the sum of torques in the vertical plane.

$$\sum_i \tau_{ih} = \tau_{proph} - \tau_{frich} - \tau_{cable}(\varphi_h) + \tau_{hv} \tag{7}$$

$$\sum_i \tau_{iv} = \tau_{propv} - \tau_{fricv} + \tau_{vh} + \tau_{gyro} \tag{8}$$

with $\tau_{proph} = l_t F_h(\omega_h)\cos\varphi_v$ represents the propulsive force generated by the tail rotor, τ_{frich} denotes the torque due to the frictional forces, $\tau_{cable}(\varphi_h)$ refers to the torque produced by the flat cable force, the term $\tau_{hv} = k_m\dot{\omega}_v\cos\varphi_v$ as presented in Eqs (7) and (8) signifies the influence of the main propeller speed on horizontal movement, $\tau_{propv} = l_m F_v(\omega_v)$ represents the torque due to the propulsive force of the main rotor, τ_{fricv} is the torque associated with the frictional forces, $\tau_{vh} = k_t\dot{\omega}_h$ denotes the effect of the tail rotor speed on vertical movement of the beam, $\tau_{gyro} = k_g F_v(\omega_v)\dot{\omega}_h\cos\varphi_v$ represents the torque due to the gyroscopic effect. The functions $F_h(\omega_h), F_v(\omega_v)$ are defined by the following equations.

$$F_h(\omega_h) = \begin{cases} k_{fhp}|\omega_h|\omega_h & \omega_h \geq 0 \\ k_{fhn}|\omega_h|\omega_h & \omega_h < 0 \end{cases} \tag{9}$$

$$F_v(\omega_v) = \begin{cases} k_{fvp}|\omega_v|\omega_v & \omega_v \geq 0 \\ k_{fvn}|\omega_v|\omega_v & \omega_v < 0 \end{cases} \tag{10}$$

where ω_h, ω_v represent the rotational speeds of the tail rotor and main rotor, respectively.

Vector $\underline{\tau}_d$ is defined as the bounded input disturbance torque vector, as specified by Eq (11) below:

$$\underline{\tau}_d = \begin{bmatrix} -M_{frich} - M_{cable}(\varphi_h) + k_m\dot{\omega}_v\cos\varphi_v \\ -h\left(m_{T_1}l_{T_1}\sin\varphi_v - m_{T_2}l_{T_2}\cos\varphi_v\right)\ddot{\varphi}_v \\ -M_{fricv} + k_t\dot{\omega}_h + M_{gyro} \\ -h\left(m_{T_1}l_{T_1}\sin\varphi_v - m_{T_2}l_{T_2}\cos\varphi_v\right)\ddot{\varphi}_h \end{bmatrix} \tag{11}$$

with $\|\underline{\tau}_d\| < a_0 + a_1\|\underline{\varphi}\| + a_2\|\underline{\dot{\varphi}}\|^2$, it is the additive disturbances, in practice $\underline{\tau}_d$ is a disturbance vector that depends on the position, velocity, pitch, and yaw of the TRMS, and it is difficult to determine.

III. Racking Control of TRMS by Combining Non-Model Feedback Linearization Regulator and IL

A. *The Proposed Control Structure*

From equation (3), the TRMS model can be rewritten as follows:

$$\underline{\ddot{\varphi}} = -\boldsymbol{\Gamma_1}\underline{\varphi} - \boldsymbol{\Gamma_2}\underline{\dot{\varphi}} + \underline{\tau} + \underline{\phi} \tag{12}$$

where $\boldsymbol{\Gamma_1}, \boldsymbol{\Gamma_2}$ are two optional matrices and the vector $\underline{\phi}$ is of the following form:

$$\begin{aligned} \underline{\phi} = \underline{\tau}_d + \left(\boldsymbol{I_n} + \boldsymbol{M_p}(\underline{\varphi},\underline{\theta})\right)\underline{\ddot{\varphi}} \\ - \left(\boldsymbol{C}(\underline{\varphi},\underline{\dot{\varphi}},\underline{\theta}) - \boldsymbol{\Gamma_2}\right)\underline{\dot{\varphi}} \\ - \left(\boldsymbol{G}(\underline{\varphi},\underline{\theta}) - \boldsymbol{\Gamma_1}\underline{\varphi}\right) \end{aligned} \tag{13}$$

where vector $\underline{\phi}$ denotes unknown functions that characterize the nonlinear disturbances arising from factors such as frictional forces, connecting cables, the influence of the main rotor speed on horizontal movement, and the effect of the tail rotor speed on vertical movement. Utilizing the models described in Eqs (3), (12) and (13), we propose a trajectory tracking control structure for TRMS, as illustrated in Fig. 3, detailed as follows:

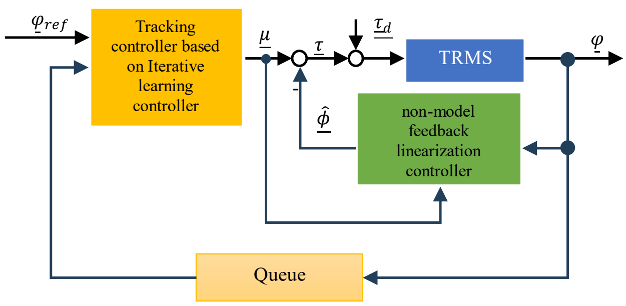

Fig. 3. Tracking control for TRMS by using non-model feedback linearization regulator and iterative learning

- Inner control loop: This loop is the linearized control loop achieved by using a compensator of the form described in equation (14) below, where $\underline{\hat{\phi}}$ is the estimate of the unknown function vector $\underline{\phi}$ in equation (13).

$$\underline{\tau} = \underline{\mu} - \underline{\hat{\phi}} \tag{14}$$

The inner closed-loop system, consisting of the TRMS system (3) and the compensator (14) will become linear according to the formula (15).

$$\begin{cases} \dot{\underline{z}} = \boldsymbol{A}\underline{z} + \boldsymbol{B}\left(\underline{\mu} + \underline{\gamma}\right) \\ \underline{y} = \underline{\varphi} = \boldsymbol{C}\underline{z} \end{cases} \tag{15}$$

where $\underline{\gamma} = \underline{\phi} - \hat{\underline{\phi}}$ is the estimation error, and

$$\underline{z} = \begin{pmatrix} \underline{\alpha} \\ \dot{\underline{\alpha}} \end{pmatrix}, \boldsymbol{A} = \begin{pmatrix} \boldsymbol{0}_2 & \boldsymbol{I}_2 \\ -\boldsymbol{\Gamma_1} & -\boldsymbol{\Gamma_2} \end{pmatrix}, \mathbf{B} = \begin{pmatrix} \mathbf{0_2} \\ I_2 \end{pmatrix}, \mathrm{C} = (\boldsymbol{I}_2, \boldsymbol{0}_2) \tag{16}$$

where $\boldsymbol{0}_2$ denotes 2×2 zero matrix, and $\boldsymbol{I}_2$ represents 2×2 identity matrix. The estimation $\hat{\underline{\phi}}$ is conducted without relying on a specific model, thereby characterizing the internal loop as a non-model-based feedback linearization loop.

- Outer control loop: This loop is designed for trajectory tracking, where the linear system described in Eq (15) is managed using an IL-based control law. The objective is to ensure that the pitch and yaw angles of TRMS, denoted as $\underline{y}$, converge to the reference angles $\underline{y}_{ref}$.

B. *Linearized Feedback Using Disturbance Compensation*

From equation (15), it is essential to design the linearization block to estimate $\hat{\underline{\phi}}(t)$ based on the measurable values of $\underline{z}(t)$ in order to compensate for $\underline{\phi}(t)$ and minimize $\underline{\gamma}(t)$, if $\hat{\underline{\phi}}(t) = \underline{\phi}(t)$ then the model described by Eq. (15) will be transformed into a linear form as indicated by Eq. (17) below:

$$\dot{\underline{z}}(t) = \boldsymbol{A}\underline{z}(t) + \boldsymbol{B}\underline{\mu}(t) \tag{17}$$

To accomplish this, consider the system at time t between the sampling instants k and $k+1$, where $t = k\Delta T + \zeta$ with $0 \le \zeta < \Delta T$, and ΔT is a sufficiently small sampling period. Within this interval, it is assumed that $\underline{\mu}_k(\zeta) = \underline{\mu}(t)$, and $\underline{z}_k(\zeta) = \underline{z}(t)$. Consequently, the system model described in Eq. (17) can be reformulated as follows:

$$\dot{\underline{z}}_k(\zeta) = \boldsymbol{A}\underline{z}_k(\zeta) + \boldsymbol{B}\left(\underline{\mu}_k(\zeta) + \underline{\phi}_k(\zeta) - \hat{\underline{\phi}}_k(\zeta)\right) \tag{18}$$

Consider $\underline{z}_k(iT_s)$ and $\underline{z}_k\big((i-1)T_s\big)$, where $0 < T_s \ll 1$ is a sufficiently small sampling interval. Here $\zeta = iT_s$ represents the current time value, and $\zeta - T_s = (i-1)T_s$ represents the preceding time value. The Taylor expansion [48], [49] of $\underline{z}_k(\zeta)$ around the point $(i-1)T_s$ allows $\underline{z}_k(\zeta)$ to be approximated by the following formula (19):

$$\underline{z}_k\big((i-1)T_s\big) = \underline{z}_k(iT_s) - T_s\, \dot{\underline{z}}_k(iT_s) + \frac{T_s^2}{2}\ddot{\underline{z}}_k(\xi) \tag{19}$$

where $(i-1)T_s \le \xi \le iT_s$, or

$$\dot{\underline{z}}_k(iT_s) \approx \frac{\underline{z}_k(iT_s) - \underline{z}_k\big((i-1)T_s\big)}{T_s} \tag{20}$$

By omitting the higher-order terms in equation (19), equation (18) can be approximated as:

$$\frac{\underline{z}_k(iT_s) - \underline{z}_k\big((i-1)T_s\big)}{T_s} \approx \boldsymbol{A}\underline{z}_k(iT_s) + \boldsymbol{B}\left(\underline{\mu}_k(iT_s) + \underline{\phi}_k(iT_s) - \hat{\underline{\phi}}_k((i-1)T_s)\right) \tag{21}$$

Replacing the symbol " ≈ "with " = ", and $\underline{\phi}_k(iT_s)$ with $\hat{\underline{\phi}}_k(iT_s)$, equation (21) becomes:

$$\frac{\underline{z}_k(iT_s) - \underline{z}_k\big((i-1)T_s\big)}{T_s} = \boldsymbol{A}\underline{z}_k(iT_s) + \boldsymbol{B}\left(\underline{\mu}_k(iT_s) + \hat{\underline{\phi}}_k(iT_s) - \hat{\underline{\phi}}_k((i-1)T_s)\right) \tag{22}$$

Thus, we have

$$\boldsymbol{B}\,\hat{\underline{\phi}}_k(iT_s) = \frac{\underline{z}_k(iT_s) - \underline{z}_k\big((i-1)T_s\big)}{T_s} - \boldsymbol{A}\underline{z}_k(iT_s) - \boldsymbol{B}\left(\underline{\mu}_k(iT_s) - \hat{\underline{\phi}}_k((i-1)T_s)\right) \tag{23}$$

Finally, the estimated value $\hat{\underline{\phi}}_k(iT_s)$ is calculated using the measured values $\underline{z}_k(iT_s)$, $\underline{z}_k\big((i-1)T_s\big)$ and the previous estimated value $\hat{\underline{\phi}}_k((i-1)T_s)$ according to the following formula:

$$\hat{\underline{\phi}}_k(iT_s) = B^T\left[\frac{\underline{z}_k(iT_s) - \underline{z}_k\big((i-1)T_s\big)}{T_s} - \boldsymbol{A}\underline{z}_k(iT_s)\right] - \left(\underline{\mu}_k(iT_s) - \hat{\underline{\phi}}_k((i-1)T_s)\right) \tag{24}$$

It is important to note that the estimator described in Eq. (24) is employed to compensate for the total disturbance vector $\underline{\phi}$ and model mismatches without relying on the original TRMS model. Consequently, the compensator detailed in Eq. (14) which utilizes $\hat{\underline{\phi}}_k(iT_s)$ as specified in Eq. (24) is also classified as a model-free compensator.

Theorem 1: *For the model described in Eq.* (12)*, the estimate* $\hat{\underline{\phi}}_k(iT_s)$ *derived from Eq* (24) *will minimize the approximation error associated with Eq* (21).

Proof: *Let the error* $\underline{\varepsilon}$ *between the two sides of equation* (21) *as indicated by Eq* (24) *below*

$$\underline{\varepsilon} = \boldsymbol{A}\underline{z}_k(iT_s) + \boldsymbol{B}\left(\underline{\mu}_k(iT_s) + \underline{\phi}_k(iT_s) - \hat{\underline{\phi}}_k((i-1)T_s)\right) - \frac{\underline{z}_k(iT_s) - \underline{z}_k\big((i-1)T_s\big)}{T_s} = \boldsymbol{B}\underline{\phi}_k(iT_s) + \underline{\gamma} \tag{25}$$

With

$$\underline{\gamma} = \boldsymbol{A}\underline{z}_k(iT_s) + \boldsymbol{B}\left(\underline{\mu}_k(iT_s) - \hat{\underline{\phi}}_k((i-1)T_s)\right) - \frac{\underline{z}_k(iT_s) - \underline{z}_k\big((i-1)T_s\big)}{T_s} \tag{26}$$

then the following minimization problem

$$\begin{aligned} \boldsymbol{\phi}^* &= \underset{\underline{\phi}_k}{\operatorname{argmin}} \|\boldsymbol{\epsilon}\|^2 \\ &= \underset{\underline{\phi}_k}{\operatorname{argmin}} \left\|\boldsymbol{B}\underline{\phi}_k + \underline{\gamma}\right\|^2 \\ &= \underset{\underline{\phi}_k}{\operatorname{argmin}} \left[\boldsymbol{B}\underline{\phi}_k + \gamma\right]^{\boldsymbol{T}} \left[\boldsymbol{B}\underline{\phi}_k + \underline{\gamma}\right] \\ &= \underset{\underline{\phi}_k}{\operatorname{argmin}} \left[\underline{\phi}_k^T\underline{\phi}_k + 2\underline{\gamma}^T\boldsymbol{B}\underline{\phi}_k + \underline{\gamma}^T\underline{\gamma}\right] \end{aligned} \tag{27}$$

has a unique solution

$$\boldsymbol{\phi}^* = -\boldsymbol{B}^T \underline{\gamma} \tag{28}$$

which ensures $\underline{\hat{\phi}}_k(iT_s)$ as given in equation (24).

C. *Linearization of Feedback Using Non-Model-Based Compensation*

Once the total disturbance $\underline{\phi}$, as defined in (13), is compensated for using Eq. (14), the system described by Eq. (12) transforms into a linear time-invariant (LTI) system [44]-[47] as characterized by Eq. (15), This system is represented in the form of ILC as follows

$$\begin{cases} \underline{z}_k(i+1) = \widehat{\boldsymbol{A}}\underline{z}_k(i) + \widehat{\boldsymbol{B}}\left[\underline{\mu}_k(i) + \underline{\gamma}_k(i)\right] \\ \underline{y}_k(i) = \boldsymbol{C}\underline{z}_k(i) \end{cases} \tag{29}$$

where $i = 0,1,\dots,N = T/T_s$, $\underline{z}_k(N) = \underline{z}_{k+1}(0)$, $\widehat{\boldsymbol{A}} = e^{AT_s}$, $\widehat{\boldsymbol{B}} = \int_0^{T_s} e^{AT_s}\boldsymbol{B}dt$, and $\boldsymbol{C} = (\mathbf{I_n}, \mathbf{0_n})$.

Assuming that the matrices $\boldsymbol{\Gamma_1}$ and $\boldsymbol{\Gamma_2}$ are selected such that the matrix $\boldsymbol{A}$ in Eq. (16) is Hurwitz [50], [51].

Therefore, system (15) is linear with poles located on the left side of the imaginary axis, ensuring that the internal closed-loop system is always stable. Consequently, we can proceed to design the trajectory tracking controller for the outer loop. Since the subsystem is linear and stable, the design process for the outer controller only requires a proportional controller that can be adjusted through iterative learning over a sampling period k. Specifically, the subsequent step in the control design process is to determine the parameter $\boldsymbol{K}$ for the proportional (P-type) update law.

$$\underline{\mu}_{k+1}(i) = \underline{\mu}_k(i) + \boldsymbol{K}\underline{e}_k(i) \tag{30}$$

where $\underline{e}_k(i) = \underline{y}_k^{ref}(i) - \underline{y}_k(i)$, and convergence condition requires that $\left\|\underline{e}_k(i)\right\|$ approaches zero, or at the very least, becomes as close to zero as possible.

Since $\underline{\mu}_k(i)$ is derived from ILC as described in Eq. (30) over a sufficiently small time interval, the discrete system represented by Eq. (29) is equivalent to the continuous model given by Eq. (15). Moreover, this model (29) does not incorporate any information from the TRMS system defined by Eq. (3). It can be observed from Eq. (29) that this equivalence is achievable under the assumption that $\underline{\gamma}_k(i) = 0$.

$$\underline{y}_{k+1}(i) = \boldsymbol{C}\widehat{\boldsymbol{A}}^i\,\underline{z}_k(0) + \sum_{j=0}^{i-1}\boldsymbol{C}\,\widehat{\boldsymbol{A}}^{i-i-1}\widehat{\boldsymbol{B}}\underline{\mu}_{k+1}(j) \tag{31}$$

Based on Eq. (31) and the observed ability to repeat $\underline{z}_k(0) = \underline{z}_{k+1}(0)$, for all k, we have,

$$\begin{aligned} \underline{e}_k(i) &= \underline{y}_k^{ref}(i) - \Big[\boldsymbol{C}\widehat{\boldsymbol{A}}^i\,\underline{z}_k(0) + \\ &\textstyle\sum_{j=0}^{i-1}\boldsymbol{C}\,\widehat{\boldsymbol{A}}^{i-i-1}\widehat{\boldsymbol{B}}\left(\underline{\mu}_{k+1}(j) + \boldsymbol{K}\underline{e}_k(j)\right)\Big] \\ &= \underline{y}_k^{ref}(i) - \underline{y}_k(i) - \textstyle\sum_{j=0}^{i-1}\boldsymbol{C}\,\widehat{\boldsymbol{A}}^{i-i-1}\widehat{\boldsymbol{B}}\boldsymbol{K}\underline{e}_k(j) \\ &= \left(I - \boldsymbol{C}\widehat{\boldsymbol{B}}\boldsymbol{K}\right)\underline{e}_k(i) - \textstyle\sum_{j=0}^{i-2}\boldsymbol{C}\,\widehat{\boldsymbol{A}}^{i-i-1}\widehat{\boldsymbol{B}}\boldsymbol{K}\underline{e}_k(j) \end{aligned} \tag{32}$$

Or

$$\begin{pmatrix} \underline{e}_{k+1}(0) \\ \underline{e}_{k+1}(1) \\ \vdots \\ \underline{e}_{k+1}(N-1) \end{pmatrix} = \begin{pmatrix} I - \boldsymbol{C}\widehat{\boldsymbol{B}}\boldsymbol{K} & \mathbf{0} & \dots & \mathbf{0} \\ -\boldsymbol{C}\widehat{\boldsymbol{A}}\widehat{\boldsymbol{B}}\boldsymbol{K} & I - \boldsymbol{C}\widehat{\boldsymbol{B}}\boldsymbol{K} & \cdots & \mathbf{0} \\ \vdots & \vdots & \ddots & \vdots \\ -\boldsymbol{C}\widehat{\boldsymbol{A}}^{N-1}\widehat{\boldsymbol{B}}\boldsymbol{K} & -\boldsymbol{C}\widehat{\boldsymbol{A}}^{N-2}\widehat{\boldsymbol{B}}\boldsymbol{K} & \cdots & I - \boldsymbol{C}\widehat{\boldsymbol{B}}\boldsymbol{K} \end{pmatrix} \begin{pmatrix} \underline{e}_k(0) \\ \underline{e}_k(1) \\ \vdots \\ \underline{e}_k(N-1) \end{pmatrix} \tag{33}$$

Finally, we have

$$\boldsymbol{E}_{k+1} = \Phi\boldsymbol{E}_k \tag{34}$$

With

$$\boldsymbol{E}_k = \begin{pmatrix} \underline{e}_k(0) \\ \underline{e}_k(1) \\ \vdots \\ \underline{e}_k(N-1) \end{pmatrix} \text{và } \boldsymbol{\Phi} = \begin{pmatrix} I - \boldsymbol{C}\widehat{\boldsymbol{B}}\boldsymbol{K} & \mathbf{0} & \dots & \mathbf{0} \\ -\boldsymbol{C}\widehat{\boldsymbol{A}}\widehat{\boldsymbol{B}}\boldsymbol{K} & I - \boldsymbol{C}\widehat{\boldsymbol{B}}\boldsymbol{K} & \cdots & \mathbf{0} \\ \vdots & \vdots & \ddots & \vdots \\ -\boldsymbol{C}\widehat{\boldsymbol{A}}^{N-1}\widehat{\boldsymbol{B}}\boldsymbol{K} & -\boldsymbol{C}\widehat{\boldsymbol{A}}^{N-2}\widehat{\boldsymbol{B}}\boldsymbol{K} & \cdots & I - \boldsymbol{C}\widehat{\boldsymbol{B}}\boldsymbol{K} \end{pmatrix} \tag{35}$$

***Theorem 2**: For the case where $\underline{\gamma}_k(i) = 0$, the condition $\left\|\underline{e}_k(i)\right\| \to 0$ for all $i = 0, 1, \dots, N-1$ will be met if and only if the proportional (P-type) learning parameter $\boldsymbol{K}$ is selected such that the matrix $\boldsymbol{\Phi}$, as defined in Eq.* (35), *is Schur.*

***Proof:** It is well-established that the stability of the autonomous system described by Eq.* (15) *is guaranteed if and only if the matrix* $\boldsymbol{\Phi}$ *is Schur, as previously demonstrated.*

D. *Control Algorithm and Quality of the Closed-Loop System*

To implement the proposed model-free controller as defined in Eq. (14), with $\underline{\mu}$ and $\underline{\phi}$ derived from Eq. (30) and (24), respectively, the following algorithm is established. In this control algorithm, each iteration of the while loop represents an experimental cycle, corresponding to a repeating time interval T of TRMS. This section will conclude with a general evaluation of the output tracking performance of the closed-loop system, as depicted in Fig. 3, under the condition where $\underline{\gamma}_k(i) \neq 0$.

***Theorem 3:** If the disturbance vector $\underline{\tau}_d$ is continuous and bounded, then the model-free control framework depicted in Fig. 2, which incorporates the linearization feedback block through the disturbance compensator described in Equations* (14) *and* (24) *along with the ILC block from Eq* (30) *will drive trajectory tracking error $\left\|\underline{e}_k(i)\right\|$ of TRMS to a region O around the origin. Furthermore, the radius of the attractive region O decreases as the sampling interval T_s becomes smaller.*

***Proof:** Given that $\underline{\tau}_d$ is continuous and bounded, it follows that the total disturbance $\underline{\phi}$ is also continuous and bounded. Consequently, $\underline{\gamma}$ is likewise bounded. Let κ represent the upper bound of $\underline{\gamma}$, according to Theorem 1, this upper bound can be made arbitrarily small by decreasing T_s. The validity* *of the correctness of Eq* (36) *is further supported by Theorem 2.*

$$\underline{\dot{g}} = \boldsymbol{A}\underline{g} + \boldsymbol{B}\underline{\mu} \text{ với } \underline{g} = vec(\underline{\alpha}, \underline{\dot{\alpha}}) \quad (36)$$

Subtracting (36) from (15), we have

$$\underline{\dot{\epsilon}} = \boldsymbol{A}\underline{\epsilon} - \boldsymbol{B}\underline{\gamma} \text{ with } \underline{\epsilon} = vec(\underline{e}, \underline{\dot{e}}) \quad (37)$$

Since $\mathbf{A}$ is a Hurwitz matrix, the Lyapunov equation $\mathbf{A}^T\mathbf{P} + \mathbf{PA} = -\mathbf{Q}$, where $\mathbf{Q}$ is a positive definite matrix, always has a positive definite solution $\mathbf{P}$. Utilizing the positive definite function $V(\underline{\epsilon}) = \underline{\epsilon}^T\mathbf{P}\underline{\epsilon}$, we have

$$\begin{aligned} \dot{V} &= \left(\boldsymbol{A}\underline{\epsilon} - \boldsymbol{B}\delta\right)^T \boldsymbol{P}\underline{\epsilon} + \underline{\epsilon}^T\boldsymbol{P}\left(\boldsymbol{A}\underline{\epsilon} - \boldsymbol{B}\underline{\gamma}\right) \\ &= \underline{\epsilon}^T(\boldsymbol{A}^T P + \boldsymbol{PA})\underline{\epsilon} - 2\underline{\epsilon}^T\boldsymbol{PB}\underline{\gamma} \\ &= -\underline{\epsilon}^T\boldsymbol{Q}\underline{\epsilon} - 2\underline{\epsilon}^T\boldsymbol{PB}\underline{\gamma} \\ &\le -\lambda_{max}(\boldsymbol{Q})\|\underline{\epsilon}^2\| + 2\|\boldsymbol{PB}\|\kappa\|\underline{\epsilon}\| \\ &= \|\underline{\epsilon}\|[-\lambda_{max}(\boldsymbol{Q})\|\underline{\epsilon}\| + 2\|\boldsymbol{PB}\|\kappa] \end{aligned} \quad (38)$$

where $\lambda_{max}(\mathbf{Q})$ denotes the largest eigenvalue of the positive definite matrix $\mathbf{Q}$. Since $\dot{V} < 0$ whenever.

$$2\|\boldsymbol{PB}\|\kappa < \lambda_{max}(\boldsymbol{Q})\|\kappa\| \text{ hay } \frac{2\|\boldsymbol{PB}\|\Delta}{\lambda_{max}(\boldsymbol{Q})} < \|\kappa\| \quad (39)$$

The tracking error vector $\underline{\epsilon}$ will converge towards the origin and eventually reach the attractive region defined by.

$$O = \left\{\underline{\epsilon} \in R^{2n} \left| \|\underline{\epsilon}\| \le \frac{2\|\boldsymbol{PB}\|\kappa}{\lambda_{max}(\boldsymbol{Q})} \right.\right\} \quad (40)$$

Proof completed.

IV. SIMUALTION AND EXPERIMENTAL RESULTS

In this section, we present the simulation and experimental results obtained by applying the tracking Control using feedback linearization regulator and IL for real TRMS with the physical and defined parameters listed in the appendix. Simulations were conducted using Matlab-Simulink R2020 [59]-[62], while experiments were performed with Simulink Real-Time and dSPACE 1103 hardware [56]-[58]. The experimental system utilizes additional graphical tools such as LabView running concurrently with Simulink Real-Time for data collection and plotting. The computer configuration used is a Core i5 with 16GB of RAM, and all other software is turned off during the experiment, with only Simulink Real-Time and LabView 2021 running. The initial conditions for the pitch and yaw angles are kept constant, with a sampling time of 0.01s for the inner loop and 0.1s for the outer loop. The friction torques for the two channels were determined as follows:

$$\begin{aligned} \tau_{frich} &= sign(\dot{\alpha}_h)(0.03 \times |\dot{\alpha}_h| + 3 \times 10^{-4}) \ (Nm) \\ \tau_{fricv} &= sign(\dot{\alpha}_v)(0.0024 \times |\dot{\alpha}_v| + 5.69 \times 10^{-4}) \ (Nm) \end{aligned} \quad (41)$$

The cable torque was determined using:

$$\tau_{cable} = 0.0016 \times (\alpha_h + 0.0002) \ (Nm) \quad (42)$$

The tracking control algorithm for the TRMS, employing feedback linearization and ILC, is generalized as follows.

Algorithm of tracking control for TRMS by using feedback linearization regulator and IL

Initialization:
Choose $\boldsymbol{\Gamma_1}, \boldsymbol{\Gamma_2}$ so that matrix $\boldsymbol{A}$ is Hurwitz
Choose the constant T_s to be sufficiently small
Calculate $N = T/T_s$
Calculate $\widehat{\boldsymbol{A}}, \widehat{\boldsymbol{B}}$
Choose the initial value of $\underline{\hat{\phi}}$
Choose matrix $\boldsymbol{K}$ so that matrix $\boldsymbol{\Phi}$ is Schur
while not stop **do**
  for $i = 0,1,2,\dots,N$ **do**
    Send out the control signal $\underline{\tau} = \underline{\mu} - \underline{\hat{\phi}}$ to TRMS during T_s
    Measure $\underline{y}(i) = \underline{\varphi} = [\varphi_h \quad \varphi_v]^T$, $\underline{\dot{\varphi}} = [\dot{\varphi}_h \quad \dot{\varphi}_v]^T$
    Calculate $\underline{e}_k(i) = \underline{y}_k^{ref}(i) - \underline{y}_k(i)$
    Calculate $\underline{\hat{\phi}} \leftarrow B^T\left[\frac{x-z}{T_s} - \boldsymbol{A}\underline{z}_k(iT_s)\right] - \left(\underline{\mu}_k(iT_s) - \underline{\hat{\phi}}_k((i-1)T_s)\right)$
    Set $\boldsymbol{x} \leftarrow z$
  end for
  Calculate $\underline{\mu}_k(i), \underline{e}_k(i)$
  $\underline{\mu}_{k+1}(i) \leftarrow \underline{\mu}_k(i) + \boldsymbol{K}\underline{e}_k(i)$
end while

To simulate and test the control algorithm, we chose square waveforms for the horizontal and vertical desired trajectories, with an amplitude of 0.4 rad, a period of 30 seconds, and a duty cycle of 50%. The initial values of α_h and α_v are 0.4 rad and -0.5 rad, respectively. The selected trajectories are well-suited to demonstrate the effectiveness of the trajectory tracking performance of the controller examined in this study. Fig. 4 through Fig. 11 present the results from both simulation and experimental tests.

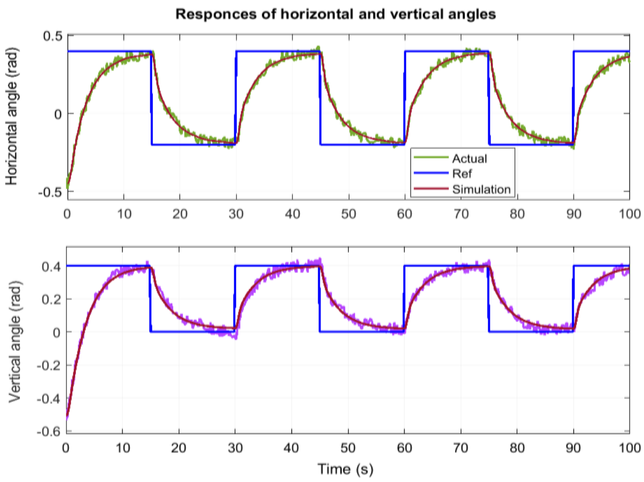

Fig. 4. Responces of horizontal and vertical angles

Fig. 4 shows the horizontal and vertical angle responses of the two cases, comparing the simulation results with the experimental results against the desired trajectory. The settling time is 10 seconds, and the overshoot is 0%. Fig. 5 illustrates the error of the experimental trajectory compared to the desired trajectory for both angles of TRMS.

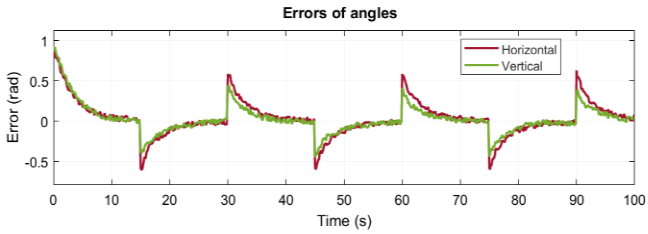

Fig. 5. Errors of horizontal and vertical angles

Fig. 6 shows the total moments acting on the TRMS for both horizontal and vertical movements, including moments from the propulsive force of the motors, friction force, flat cable force, the torque of the gyroscopic, and other forces.

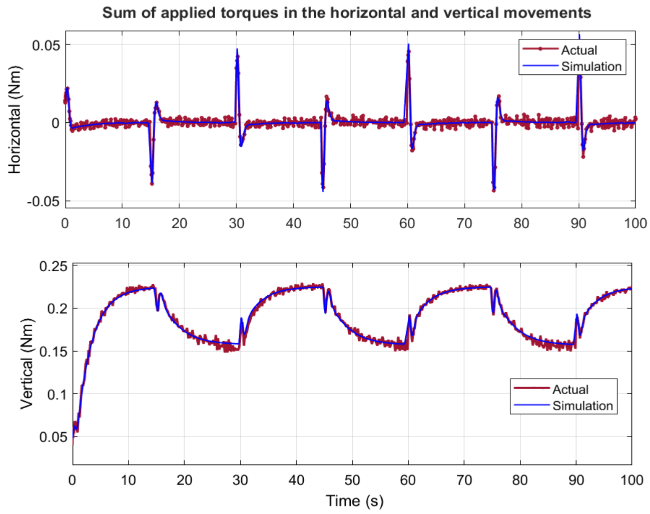

Fig. 6. Sum of the applied torques in both the horizontal and vertical directions

The control forces of horizontal and vertical angles driven by feedback linearization regulator and iterative learning are depicted in Fig. 7.

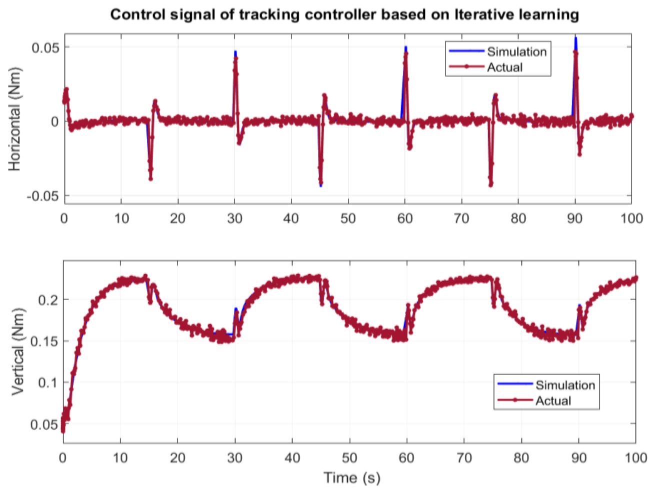

Fig. 7. Control signal of tracking controller based on iterative learning

Fig. 8 illustrates the nonlinear disturbances modeled by Eq. (24) affecting the motion of the horizontal and vertical angles, compared for both simulation and experimental cases.

Similarly, Fig. 9 presents input torque disturbances τ_d. Fig. 10 and Fig. 11 respectively depict the rotor speed and its derivative of the vertical rotor and horizontal rotor, compared between simulation and experimental results.

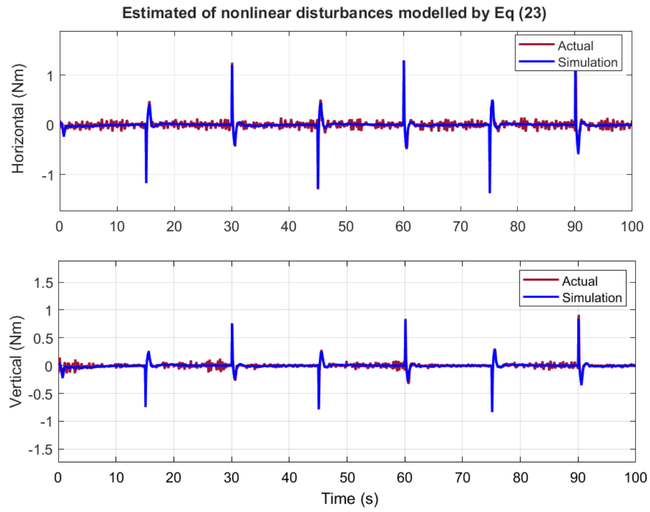

Fig. 8. Estimated of nonlinear disturbances modelled by Eq (23)

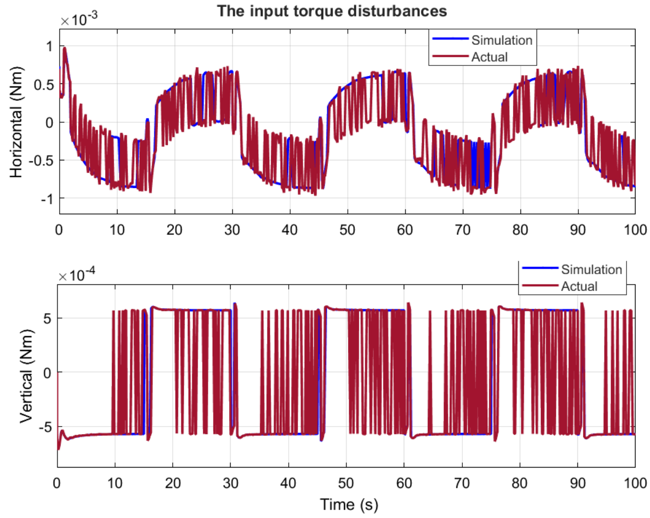

Fig. 9. The input torque disturbances

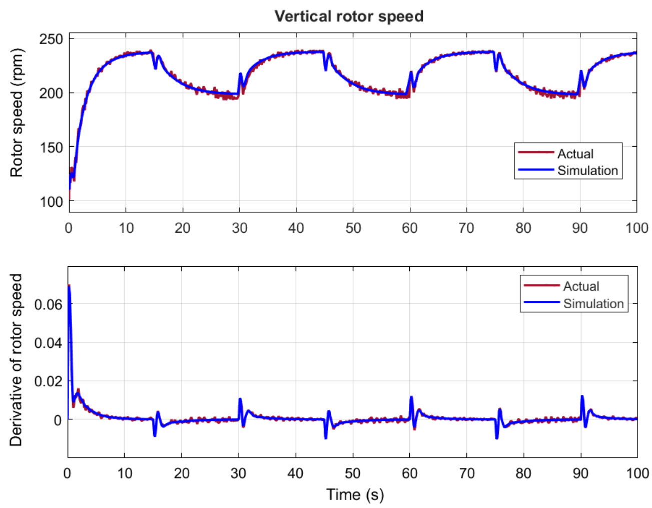

Fig. 10. Vertical rotor speed and its derivative

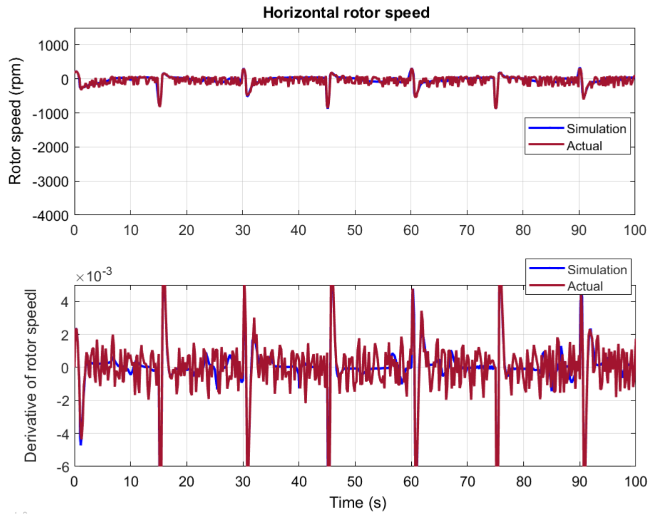

Fig. 11. Horizontal rotor speed and its derivative

The simulation and experimental results demonstrate that the trajectory tracking control system for the TRMS achieves robustness against disturbances τ_d arising during changes in pitch and yaw angles to ensure movement along the desired trajectory. At times when the desired trajectory undergoes sudden level changes, the trajectory is smoothly adjusted without amplitude spikes. This indicates that the IL controller appropriately adjusts the gain factor with each sampling cycle.

From the comparison results between the simulations and experiments, it is evident that they are consistent with each other. These results reflect the accuracy of the proposed algorithm in this paper. The compensation unit has calculated the deviation between the nonlinear noisy model of TRMS (3) and the linear model (15) to correct for this influence. The trajectory tracking controller based on IL has computed the control signals for the main and tail motors to ensure that the TRMS's pitch and yaw angles follow the desired setpoint.

V. Conclusions

This paper introduced an innovative intelligent control strategy for TRMS. The proposed controller features two main components: a disturbance compensator operating as a model-free feedback linearization regulator and an output tracking controller utilizing ILC. The model-free controller developed in this study operates independently of the traditional Euler-Lagrange model of the TRMS. Instead, it relies solely on real-time measurements of horizontal and vertical angles, making it both robust and adaptable to changing conditions without the need for an explicit dynamic model of the TRMS.

The essence of the proposed method lies in its capacity to compensate for disturbances and achieve accurate output tracking through adaptive mechanisms inherent in the model-free framework. The disturbance compensator is specifically designed to address uncertainties and matched disturbances, thereby ensuring stable and precise control. Concurrently, the output tracking controller, derived from the ILC paradigm, improves performance by iteratively refining control actions based on previous tracking errors. This iterative process enhances accuracy and facilitates convergence to desired tracking objectives. The advantage of the method mentioned in this study lies in its ability to compensate for the nonlinear characteristics of the TRMS using a feedback linearization controller, where the estimated nonlinear component deviations are considered as input disturbances of the linear system with known system matrices. Although the computational load is quite large compared to other control methods, with modern microprocessors, this can be easily implemented in commercial systems. Simulation and experimental results confirm that the proposed intelligent model-free controller demonstrates exceptional adaptive performance, consistent with expected outcomes. These results validate the controller's effectiveness in managing uncertainties and achieving accurate output tracking, underscoring its potential for practical applications in robotics.

Our future work is to simplify the determination of the feedback linearization controller and the trajectory tracking controller using IL to reduce computational load. This will further enhance robustness against external influences, such as wind blowing on the TRMS from different directions, impacting the TRMS.

VI. Appendix

The physical parameters provided by Feedback Instruments Limited (Table I), along with the defined parameters of TRMS.

TABLE I. The Physical Parameters Supplied by the Feedback Instrument

Symbol	Quantity	Value
m_b	Mass of the counter-weight beam	0.022kg
m_{cb}	Mass of the counter-weight	0.068kg
m_m	Mass of main part of the beam	0.014kg
m_{mr}	Mass of the main DC motor	0.236kg
m_{ms}	Mass of the main shield	0.219kg
m_t	Mass of the tail part of the beam	0.015kg
m_{tr}	Mass of the tail DC motor	0.221kg
m_{ts}	Mass of the tail shield	0.119kg
r_{ms}	Radius of the main shield	0.155m
r_{ts}	Radius of the tail shield	0.1m
h	Length of the offset between base and joint	0.06m
g	Gravitational acceleration	9.8m/s^2
k_g	Gyroscopic constant	0.2
k_m	Positive constant	2×10^{-4}
k_t	Positive constant	2.6×10^{-5}
l_t	Length of tail part of the beam	0.282m
l_m	Length of main part of the beam	0.246m
l_b	Length of counter-weight beam	0.29m
l_{cb}	Distance between counterweight and joint	0.276m
k_{fhp}	Positive constant	1.84×10^{-6}
k_{fhn}	Positive constant	2.2×10^{-7}
k_{fvp}	Positive constant	1.62×10^{-5}
k_{fvn}	Positive constant	1.08×10^{-5}

The defined parameters of TRMS model:

$$\begin{aligned} m_{T_1} &= m_t + m_{tr} + m_{ts} + m_m + m_{mr} + m_{ms} \\ m_{T_2} &= m_b + m_{cb} \\ l_{T_1} &= \frac{(0.5m_m + m_{mr} + m_{ms})l_m - (0.5m_t + m_{tr} + m_{ts})l_t}{m_{T_1}} \end{aligned} \tag{43}$$

$$l_{T_2} = \frac{0.5m_b l_b + m_{cb} l_{cb}}{m_{T_2}}$$

$$J_1 = \left(\frac{m_t}{3} + m_{tr} + m_{ts}\right) l_t^2 + \left(\frac{m_m}{3} + m_{mr} + m_{ms}\right) l_m^2 + \frac{m_{ms}}{2} r_{ms}^2 + m_{ts} r_{tr}^2$$

$$J_2 = \frac{m_b}{3} l_b^2 + m_{cb} l_{cb}^2, J_3 = \frac{m_h}{3} h^2$$

ACKNOWLEDGMENT

This research was supported by the Research Foundation funded by the Thai Nguyen University ofTechnology.

REFERENCES

[1] TRMS 33-949S, *User Manual*. Feedback instruments Ltd., East Sussex, U. K, 1998.

[2] S. K. Pandey, J. Dey, and S. Banerjee, "Design and real-time implementation of robust PID controller for Twin Rotor MIMO System (TRMS) based on Kharitonov's theorem," in IEEE *1st International Conference on Power Electronics, Intelligent Control and Energy Systems* (ICPEICES), pp. 1-6, 2016, doi: 10.1109/ICPEICES.2016.7853106.

[3] A. A. Patel, P. M. Pithadiya, and H. V. Kannad, "Control of Twin Rotor MIMO System (TRMS) Using PID Controller," in *National Conference on Emerging Trends in Computer, Electrical & Electronics (ETCEE-2015) International Journal of Advance Engineering and Research Development (IJAERD)*, pp. 2348-4470, 2015.

[4] Fahmizal, H. A. Nugroho, A. I. Cahyadi and I. Ardiyanto, "Twin Rotor MIMO System Control using Linear Quadratic Regulator with Simechanics," in 7th *International Conference on Electrical, Electronics and Information Engineering (ICEEIE)*, pp. 301-306, 2021, doi: 10.1109/ICEEIE52663.2021.9616893.

[5] A. Rahideh and M. H. Shaheed, "Mathematical dynamic modelling of a twin-rotor multiple input-multiple output system," in *Proceedings of the Institution of Mechanical Engineers, Part I: Journal of Systems and Control Engineering*, vol. 221, no. 1, pp. 89-101, 2007.

[6] A. K. Ekbote, N. S. Srinivasan, and A. D. Mahindrakar, "Terminal sliding mode control of a Twin rotor multiple-input multiple Output System," *IFAC Proceedings Volumes*, vol. 44, no. 1, pp. 10952-10957, 2011.

[7] S. Sajjad Moosapour, H. Mehdipour, and M. Keramatzadeh, "Sliding Mode Disturbance Observer-Based Control of a Laboratory Twin Rotor Multi Input-Multi Output System," in *IEEE Access*, vol. 13, pp. 394-406, 2025, doi: 10.1109/ACCESS.2024.3523850.

[8] B. Loutfi, Z. Samir, D. Ali, and G. M. Zinelaabidine, "Real time implementation of type-2 fuzzy backstepping sliding mode controller for twin rotor MIMO system (TRMS)," *Traitement du Signal*, vol. 36, no. 1, pp. 1-11, 2019.

[9] M. Derakhshannia, S. B. F. Asl, and S. S. Moosapour, "Backstepping Terminal Sliding Mode Control Design for a TRMS," *2021 7th International Conference on Control, Instrumentation and Automation (ICCIA)*, pp. 1-5, 2021, doi: 10.1109/ICCIA52082.2021.9403545.

[10] N. Abbas, Z. Abbas, and X. Liu, "Adaptive recursive sliding mode control (ARSMC)-Based UAV control for future smart cities," in *Applied Sciences*, vol. 13, no. 11, pp. 6790, 2023.

[11] X. Yang *et al.*, "Input shaping enhanced active disturbance rejection control for a twin rotor multi-input multi-output system (TRMS)," in *ISA transactions*, vol. 62, pp. 287-298, 2016.

[12] G. Shivani, A. Jamodkar, and B. J. Pandian, "Modeling and Implementation of Adaptive Control Technique on a TRMS Model," in *International Journal of Innovative Technology and Exploring Engineering*, vol. 8, no. 8, pp. 1015-1020, 2019.

[13] A. Rahideh, M. H. Shaheed, and A. H. Bajodah, "Adaptive Nonlinear Model Inversion Control of a Twin Rotor System Using Artificial Intelligence," in *IEEE International Conference on Control Applications*, pp. 898-903, 2007, doi: 10.1109/CCA.2007.4389347.

[14] F. Faris, A. Moussaoui, B. Djamel, and T. Mohammed, "Design and real-time implementation of a decentralized sliding mode controller for twin rotor multi-input multi-output system," in *Proceedings of the Institution of Mechanical Engineers, Part I: Journal of Systems and Control Engineering*, vol. 231, no. 1, pp. 3-13, 2017, doi: 10.1177/0959651816680457

[15] E. S. Ghith and F. A. A. Tolba, "Design and optimization of PID controller using various algorithms for micro-robotics system," in *Journal of Robotics and Control (JRC)*, vol. 3, no. 3, pp. 244-256, 2022.

[16] M. H. Shaheed, "Feedforward neural network based non-linear dynamic modelling of a TRMS using RPROP algorithm," in *Aircraft Engineering and Aerospace Technology*, vol. 77, no. 1, pp. 13-22, 2005.

[17] A. Rahideh, M. H. Shaheed, and H. J. C. Huijberts, "Dynamic modelling of a TRMS using analytical and empirical approaches," in *Control Engineering Practice*, vol. 16, no. 3, pp. 241-259, 2008.

[18] G. S. Rao *et al.*, "Evaluating and optimizing surface roughness using genetic algorithm and artificial neural networks during turning of AISI 52100 steel," *in International Journal on Interactive Design and Manufacturing (IJIDeM)*, vol. 18, no. 8, pp. 6151-6160, 2024.

[19] M. H. Shaheed, "Performance analysis of 4 types of conjugate gradient algorithms in the nonlinear dynamic modelling of a TRMS using feedforward neural networks," *2004 IEEE International Conference on Systems, Man and Cybernetics (IEEE Cat. No.04CH37583)*, vol. 6, pp. 5985-5990, 2004, doi: 10.1109/ICSMC.2004.1401153.

[20] A. Jain, S. Sheel, and P. Kuchhal, "Fuzzy logic-based real-time control for a twin-rotor MIMO system using GA-based optimization," *World Journal of Engineering*, vol. 15, no. 2, pp. 192-204, 2018.

[21] S. Bandyopadhyay, P. Pramanick, and C. Dey, "Fuzzy Rule-Based supervisory PID Auto-Tuner for TRMS process," in *Proceedings of the Fourth International Conference on Microelectronics, Computing and Communication Systems: MCCS 2019*, pp. 655-669, 2021.

[22] S. K. Valluru, R. Kumar, and R. Kumar, "Design and Real Time implementation of fmincon, MOGA tuned IO-PID and FO-PIλDμ Controllers for Stabilization of TRMS," in *Procedia Computer Science*, vol. 171, pp. 1241-1250, 2020.

[23] K. Kalyani and S. Kanagalakshmi, "Control of Trms using Adaptive Neuro Fuzzy Inference System (ANFIS)," *2020 International Conference on System, Computation, Automation and Networking (ICSCAN)*, pp. 1-5, 2020, doi: 10.1109/ICSCAN49426.2020.9262417.

[24] F. L. Lewis, D. M. Dawson, and C. T. Abdallah, *Robot manipulator control: theory and practice*. CRC Press, 2003.

[25] E. D. Sontag and Y. Wang, "On characterizations of the input-to-state stability property," *Systems & Control Letters*, vol. 24, no. 5, pp. 351-359, 1995.

[26] N. V. Chi and N. D. Phuoc, "Adaptive tracking control based on disturbance attenuation and ISS stabilization of Euler-Lagrange nonlinear in the presence of uncertainty and input noise," in *Proceedings of IEEE 2th Int. Conference on Electrical Engineering and Automation Control (EEAC2011)*, pp. 3698-3071, 2011.

[27] N. V. Chi, "Adaptive feedback linearization control for twin rotor multiple-input multiple-output system," in *Int. J. Control Autom. Syst.*, vol. 15, pp. 1267–1274, 2017.

[28] N. V. Chi, "Adaptive sliding mode tracking control for twin rotor multi-input multi-output nonlinear system," in *Int. J. Control Autom. Syst.*, vol. 4, no. 4, pp. 9-16, 2015.

[29] D. U. Rijalusalam and I. Iswanto, "Implementation kinematics modeling and odometry of four omni wheel mobile robot on the trajectory planning and motion control based microcontroller," in *Journal of Robotics and Control (JRC)*, vol. 2, no. 5, pp. 448-455, 2021.

[30] J. H. Pérez-Cruz, "Stabilization and synchronization of uncertain zhang system by means of robust adaptive control," in *Complexity*, vol. 2018, no. 1, pp. 4989520, 2018.

[31] C. N. Van and P. N. Doan, "Adaptive ISS Stabilization Tracking Control Of Nonlinear Systems In The Presence Of Uncertainty And Input Noise With Guaranteed Tracking Errors," in *Journal of Computer Science and Cybernetics*, vol. 29, no. 2, 2013.

[32] A. Rahideh and M. H. Shaheed, "Mathematical dynamic modelling of a twin-rotor multiple input-multiple output system," *Proceedings of the Institution of Mechanical Engineers, Part I: Journal of Systems and Control Engineering*, vol. 221, no. 1, pp. 89-101, 2007.

[33] D. Rotondo, F. Nejjari, and V. Puig, "Quasi-LPV modeling, identification and control of a twin rotor MIMO system," in *Control Engineering Practice*, vol. 21, no. 6, pp. 829-846, 2013.

[34] D. Rotondo, *Advances in gain-scheduling and fault tolerant control techniques*. Springer, 2017.

[35] X. Yang *et al*., "Input shaping enhanced active disturbance rejection control for a twin rotor multi-input multi-output system (TRMS)," in *ISA transactions*, vol. 62, pp. 287-298, 2016.

[36] G. Srinivasarao, A. K. Samantaray, and S. K. Ghoshal, "Cascaded adaptive integral backstepping sliding mode and super-twisting controller for twin rotor system using bond graph model," in *ISA transactions*, vol. 130, pp. 516-532, 2022.

[37] W. Perruquetti and J. P. Barbot, *Sliding mode control in engineering*. New York: Marcel Dekker, 2002.

[38] N. D. Phuoc, *Analysys and Control for nonlinear systems*. Science and Technics Publishing House, Viet Nam, 2002.

[39] H. P. Tairen Suna, Y. Pana, H. Zhoua, and C. Zhangc, “Neural network-based sliding mode adaptive control for robot manipulators,” in *Neuro computing*, vol. 74, no. 14–15, pp. 2377-2384, 2011.

[40] V. I. Utkin and A. S. Poznyak, "Adaptive sliding mode control," in *Advances in Sliding Mode Control: Concept, Theory and Implementation*, pp. 21-53, 2013.

[41] A. Allevato, M. Pryor, and A. L. Thomaz, "Multiparameter Real-World System Identification Using Iterative Residual Tuning," in *ASME. J. Mechanisms Robotics*, vol. 13, no. 3, p. 031021, 2021.

[42] E. Spyrakos-Papastavridis and J. S. Dai, "Flexible-Joint Humanoid Balancing Augmentation via Full-State Feedback Variable Impedance Control," in *ASME. J. Mechanisms Robotics*, vol. 13, no. 2, p. 021014, 2021.

[43] L. Cuvillon, X. Weber, and J. Gangloff, "Modal Control for Active Vibration Damping of Cable-Driven Parallel Robots," in *ASME. J. Mechanisms Robotics*, vol. 12, no. 5, p. 051004, 2020.

[44] M. H. H. Kani, H. A. Yaghini Bonabi, H. Jalaly Bidgoly, M. Javad Yazdanpanah, and M. Nili Ahmadabadi, "Design and Implementation of a Distributed Variable Impedance Actuator Using Parallel Linear Springs," in *ASME. J. Mechanisms Robotics*, vol. 8, no. 2, p. 021024, 2016.

[45] N. Olgac and R. Sipahi, "An exact method for the stability analysis of time-delayed linear time-invariant (LTI) systems," in *IEEE Transactions on Automatic Control*, vol. 47, no. 5, pp. 793-797, 2002.

[46] R. Goyal, G. Parmar, and A. Sikander, "A new approach for simplification and control of linear time invariant systems," in *Microsystem Technologies*, vol. 25, pp. 599-607, 2019.

[47] W. A. Malik, S. Darbha, and S. P. Bhattacharyya, "On the transient control of Linear Time Invariant systems," *2009 American Control Conference*, pp. 3142-3147, 2009, doi: 10.1109/ACC.2009.5160676.

[48] M. Pourahmadi, "Taylor expansion of and some applications," in *The American Mathematical Monthly*, vol. 91, no. 5, pp. 303-307, 1984.

[49] E. M. Wright, "The asymptotic expansion of integral functions defined by Taylor series," in *Philosophical Transactions of the Royal Society of London. Series A, Mathematical and Physical Sciences*, vol. 238, no. 795, pp. 423-451, 1940.

[50] F. J. Kraus, M. Mansour, and M. Sebek. "Hurwitz matrix for polynomial matrices," in *Stability Theory: Hurwitz Centenary Conference Centro Stefano Franscini, Ascona*, pp. 67-74, 1996.

[51] W. Li, "Practical criteria for positive-definite matrix, M-matrix and Hurwitz matrix," in *Applied mathematics and computation*, vol. 185, no. 1, pp. 397-401, 2007.

[52] D. A. Bristow, M. Tharayil, and A. G. Alleyne, "A survey of iterative learning control," in *IEEE control systems magazine*, vol. 26, no. 3, pp. 96-114, 2006.

[53] H-. S. Ahn, Y. Q. Chen, and K. L. Moore, "Iterative learning control: Brief survey and categorization," in *IEEE Transactions on Systems, Man, and Cybernetics, Part C (Applications and Reviews)*, vol. 37, no. 6, pp. 1099-1121, 2007.

[54] Z. Bien and J-. X. Xu, *Iterative learning control: analysis, design, integration and applications.* in Springer Science & Business Media, 2012.

[55] N. Amann, D. H. Owens, and E. Rogers, "Predictive optimal iterative learning control," in *International Journal of Control*, vol. 69, no. 2, pp. 203-226, 1998.

[56] R. Amalrajan, R. Gunabalan, and N. Tewari, "DSPACE1103 controller for PWM control of power electronic converters," in *Advances in Smart Grid Technology: Select Proceedings of PECCON 2019—Volume I*, pp. 307-322, 2020.

[57] T. Boutabba *et al*., "dSPACE Real-Time Implementation of Maximum Power Point Tracking Based on Kalman Filter Structure using Photovoltaic System Emulator," *2021 International Conference on Control, Automation and Diagnosis (ICCAD)*, pp. 1-6, 2021, doi: 10.1109/ICCAD52417.2021.9638743.

[58] C. B. Murugan, S. Natarajan, and R. Bensraj, "dSPACE based implementation of various inverted sine carrier PWM strategies for three phase five level H-bridge inverter," in *Int J Adv Engg Tech/Vol. VII/Issue I/Jan.-March*, vol. 103, p. 112, 2016.

[59] K. Lakomy *et al*., "Active disturbance rejection control (adrc) toolbox for matlab/simulink," in *arXiv preprint arXiv:2112.01614*, 2021.

[60] V. A. Barausov, V. P. Bubnov, and S. K. Sultonov, "Simulation modeling in methods and designs for detecting ice or snow buildup on control surface in MATLAB/SIMULINK dynamic modeling environment," in *Models and Methods for Researching Information Systems in Transport 2020 (MMRIST 2020)*, vol. 1, pp. 136-141, 2020.

[61] L. Wang, *PID control system design and automatic tuning using MATLAB/Simulink*. John Wiley & Sons, 2020.

[62] F. F. Al-Azzawi *et al*., "Modulation and RS-CC rate specifications in WiMAX IEEE 802.16 Standard with MATLAB Simulink model," in *IOP Conference Series: Materials Science and Engineering*, vol. 881, no. 1, 2020.